Carbon Nanohorns as Integrative Materials for Efficient Dye-Sensitized Solar Cells

*Rubén D. Costa, Sebastian Feihl, Axel Kahnt, Sanjeev Gambhir, David L. Offfcer, Gordon G. Wallace, María Isabel Lucio, María Antonia Herrero, Ester Vázquez, Zois Syrgiannis, Maurizio Prato, and Dirk M. Guldi**

Implementing nanocarbons, such as fullerenes, carbon nanotubes (CNTs), graphene, and carbon nanohorns (CNHs), into photovoltaic and optoelectronic applications has exciting potential, especially to achieve important and much needed breakthroughs.[1] In this context, the use of CNTs and graphene in the field of dye-sensitized solar cells (DSSCs) is currently attracting major attention, resulting in a number of recent investigations.[1a] DSSCs are among the most promising solar-energy conversion technologies, owing to their high efficiency of up to 13%,[2] low cost, simple fabrication, and ease of large-scale production.[3] However, lots of challenges remain prior to the widespread commercialization of DSSCs. These include, for example, the development of effective solid-state electrolytes, the enhancement of electronic transport in transparent photoanodes such as TiO_2 and/or ZnO, and the use of effective platinum-free counter-electrodes.[3b,4] The introduction of nanocarbons into DSSCs has emerged as a versatile strategy to take on some of these challenges. On one hand, charge injection into the semiconducting electrodes and charge transport processes across the interfaces have been improved by using either doped TiO_2 electrodes or the introduction of interlayers based on CNTs and/or graphene.[5] On the other hand, efficient quasi-solid state DSSCs have been developed with nanocarbons present in the electrolyte.[6] Importantly, several authors have recently demonstrated that DSSCs, into which graphene-based counter-electrodes have been integrated, show better performances than those using platinum-based counter-electrodes.[7] In short, the prospects of nanocarbons, in general, and CNTs and graphene, in particular, in DSSCs are clearly bright.

Among the wide variety of nanocarbons, single-walled carbon nanohorns (SWCNHs) have been largely unexplored. SWCNHs are of particular interest, owing to their semiconductor character, high porosity, and large surface areas.[1b,c] Their application is appealing because of their metal-free synthesis, by way of CO_2 laser induced ablation of graphite targets, that proceeds in high yields and high purities.[8] SWCNHs consist of tubular structures – 2 to 5 nm in diameter and 30 to 50 nm in length – that associate into roundish aggregates of 100 nm diameter. To date, their application has mainly been limited to hydrogen and methane storage, biosensing, solar thermal collectors, drug delivery systems, and supercapacitor electrodes.[1b,c,9]

It is striking that, despite their excellent properties, only a few groups have reported on their implementation into solar energy devices, such as photoelectrochemical cells.[10] Motivated by this and recent advances in DSSCs with nanocarbon/TiO_2 composites, we have explored the use of SWCNHs in TiO_2 films and compared the performances of the resulting DSSCs with those containing other nanocarbons such as graphene or SWCNTs. Our most important finding is that the presence of SWCNHs enhances the device performance when contrasted to devices that lack SWCNHs in a manner similar to that observed in other carbon-doped TiO_2-electrodes. Our investigations indicate that the roughness of the mesoporous photoelectrode, the quantity of dye adsorption, the charge transport across the electrode interface, and the charge recombination process are all impacted by the presence of SWCNHs in TiO_2-based DSSCs.

The different nanocarbon/TiO_2 composites were prepared by drop-wise addition of small amounts of nanocarbon suspensions − graphene, partially reduced graphene oxide, SWCNTs, oxidized SWCNTs, SWCNHs, and oxidized SWCNHs − to realize weight percentages of 0.1, 0.2, 0.5, and 0.7 wt%. The mixtures were continuously stirred prior to their use to ensure homogenous mixtures of all components. These composites were doctor bladed onto fluorine-doped tin oxide (FTO) substrates and successively sintered at 400 ºC for 30 min to afford the desired nanocarbon/TiO_2 photoelectrodes – see Supporting Information (SI) Section for more details.

In line with previous reports, pristine and oxidized nanocarbons present excellent thermal stability up to 450–500 °C – Figure S4.[11] For instance, pristine and oxidized SWCNHs, as they were used in the current work, are known to decompose around 900 and 600 °C, respectively.[11a] In fact, all of the

Dr. R. D. Costa, S. Feihl, Dr. A. Kahnt,
Prof. D. M. Guldi
Department of Chemistry and Pharmacy and
Interdisciplinary Center for Molecular Materials (ICMM)
Friedrich-Alexander-Universität Erlangen-Nürnberg
Erlangen, 91058, Germany
E-mail: dirk.guldi@fau.de
Dr. S. Gambhir, Prof. D. L. Officer, Prof. G. G. Wallace
Australian Research Council Centre of Excellence for Electromaterials
Science and the Intelligent Polymer Research Institute
University of Wollongong
Wollongong, NSW 2522, Australia
M. I. Lucio, Prof. M. A. Herrero, Prof. E. Vázquez
Departamento de química orgánica
facultad de químicas-IRICA
Universidad de Castilla-La Mancha
Ciudad Real, 13071, Spain
Dr. Z. Syrgiannis, Prof. M. Prato
INSTM, Unit of Trieste
Dipartimento di Scienze Farmaceutiche
Università di Trieste, Trieste, I-34127, Italy

nanocarbon/TiO_2 composites reported to date were prepared under similar conditions – vide supra.[5a–c,5h–k] Still, to ensure that heat treatment did not induce any undesired degradation processes and/or losses of nanocarbons, thermogravimetric analyses (TGAs) were performed. Figure S4 depicts typical TGA curves of composites with 0.7 wt% of nanocarbons measured in air with a ramp rate of 10 °C min^{-1}. Common to all of the TGAs is a similar weight loss profile that resembles the one seen for TiO_2 pastes lacking nanocarbons. We conclude that our composites are, indeed, very robust.

To confirm the successful incorporation of the aforementioned nanocarbons into the TiO_2 network of the electrodes, Raman assays were performed. Figure S5 displays the main Raman features of the modified and pristine electrodes from which two major conclusions were derived. On one hand, the G- and D-bands at around 1275 and 1595 cm^{-1}, respectively, are observable for the nanocarbon modified electrodes corroborating the incorporation of the latter. On the other hand, Raman peaks at 397, 517, and 639 cm^{-1} are ascribed to anatase TiO_2 nanoparticles. Importantly, no particular shifts are noted upon introducing the different nanocarbons into the films attesting that the nanocarbons are not interacting strongly with the TiO_2 nanoparticles. Further corroboration of the latter notion came from X-ray diffraction (XRD) experiments – Figure S6. In particular, a direct comparison of the XRD patterns documents that the presence of nanocarbons does not affect the nature of the anatase TiO_2 nanoparticles of around 40 nm. This finding, which is in line with the Raman experiments, strongly suggests that the incorporation of nanocarbons goes beyond simple blending and infers mutually interacting constituent.

Next, we investigated the microstructural changes that might have evolved from the implementation of nanocarbons. To shed light onto this aspect, the roughness of the different films was studied by means of desorption experiments, diffuse reflectance, and profilometry measurements, and their morphology was analyzed by means of Scanning Electron Microscopy (SEM). The roughness parameter (R) was derived in line with a previously reported method by considering the number of dye molecules adsorbed on the electrode.[5j,12] Here, R is defined as the total active surface area per unit substrate area as given by Equation (1)

$$R = D_{ad} \times N_A \times D_A \quad (1)$$

where D_{ad} is the quantity of the dye adsorption on each unit area (mol nm^{-2}), N_A is Avogadro's number, and D_A is the area per dye molecule, which is 1.6 nm^2/dye molecule (i.e., N719).[13] D_{ad} was obtained by absorption spectroscopic measurements. Importantly, the dyes were desorbed from the nanocarbon/TiO_2 photoelectrodes with 0.1 M NaOH aqueous solutions.

Table 1 summarizes all the fundamental data regarding film characterization. As it is apparent, the presence of the different nanocarbons exerts a profound impact on R. In general, upon low nanocarbon loading R increases, while higher additions lead to marked decreases of R. A likely rationale for such trends is the susceptibility of nanocarbons to agglomerate/aggregate. This leads to irregular pore sizes (i.e., low R values) and poor electrical properties of the resulting photoelectrodes (Table 1).[5a,5c,5h–k,12] Interestingly, our data suggest that the oxidized nanocarbons have a more beneficial impact on R than non-oxidized, pristine nanocarbons. Mutually interacting TiO_2 and carboxylic groups of the nanocarbons are thought to be responsible for the benefits during the heat treatment. The aforementioned is further corroborated by diffuse reflectance measurements – Figure S7, in which we are able to establish a correlation between surface roughness and light-scattering.[5i,14] Indeed, the changes in diffuse reflectance track the overall trends observed in the desorption studies and, as such, the R parameter calculations. Finally, the roughness average was calculated based on profilometry – see SI for more details. Here, the values derived from a Gaussian fitting of the surface profile indicate that the roughness is greatly increased by around

Table 1. Characterization of the different nanocarbon/TiO_2 photoelectrodes.

nanocomposite[a]	R[b]	Resistance [MΩ]	τ_{recom} [ns][d]	WF [eV][e]
single layer reference TiO_2	5.42	800[c]	36.0	4.44
SWCNH/TiO_2				
0.1	6.53	170	51.4	4.62
0.2	7.58	126	92.9	4.53
0.5	8.14	102	208	4.55
0.7	5.00	211	89.5	4.53
SWCNH$_{ox}$/TiO_2				
0.1	7.14	217	98.8	4.54
0.2	8.31	199	106	4.54
0.5	7.11	210	76.2	4.52
0.7	4.93	228	65.1	4.49
graphene/TiO_2				
0.1	6.90	115.2	146	4.55
0.2	6.35	105	57.8	4.56
0.5	6.11	78	36.8	4.55
0.7	4.63	90	36.6	4.56
graphene$_{ox}$/TiO_2				
0.1	6.13	212	36.1	4.58
0.2	6.52	217	93.4	4.62
0.5	8.04	229	127	4.61
0.7	6.28	218	64.5	4.60
SWCNT/TiO_2				
0.1	7.47	219	57.9	4.49
0.2	5.79	–	38.9	4.63
0.5	5.50	–	33.0	4.67
0.7	5.60	–	33.0	4.68
SWCNT$_{ox}$/TiO_2				
0.1	8.30	220	60.4	4.53
0.2	6.62	–	37.1	4.68
0.5	5.86	–	34.0	4.75
0.7	5.94	–	36.8	4.72

[a]data refers to electrodes doped with 0.1, 0.2, 0.5, and 0.7 wt% of the different carbon-materials; [b]R is determined by Equation (1). The data is divided by 10^2; [c]Value from reference [16]; [d]$\tau_{rec\ om}$ is the bleaching lifetime at 460 nm and is related to recombination process; [e]Work function with an error of ± 0.01 eV.

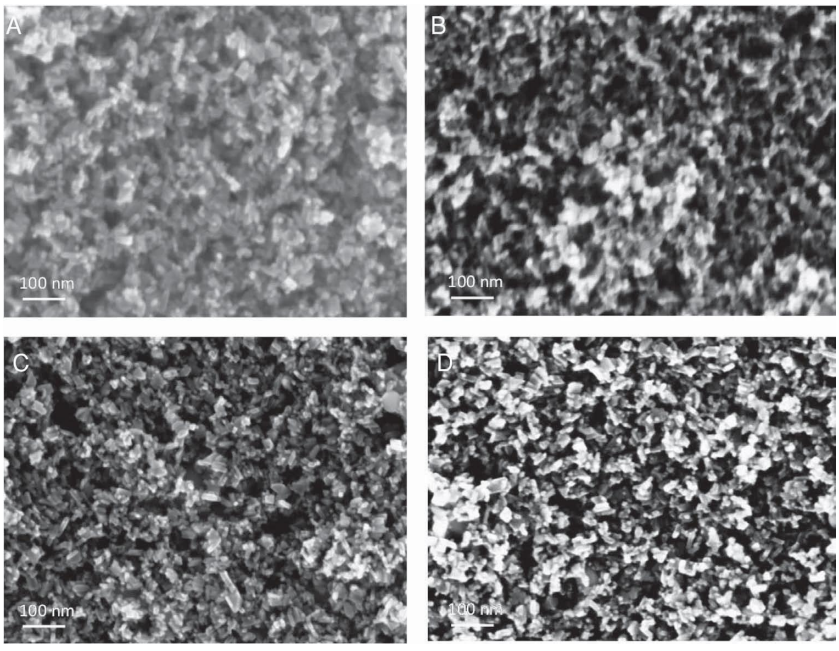

Figure 1. SEM images of SWCNH$_{ox}$/TiO$_2$ (B), Graphene$_{ox}$/TiO$_2$ (C), and SWCNT$_{ox}$/TiO$_2$ (D) films with 0.2, 0.5, and 0.1 wt%, respectively. The SEM image of the reference TiO_2 electrode (A) is also shown for comparison.

50, 45, and 15% upon implementing SWCNHs, graphene, and SWCNTs, respectively, compared to reference films.

As a rule of thumb, an increased surface roughness is related to two key features as a means to control the device performance. On one hand, it regulates the quantity of dye adsorption and, on the other hand, it increases light scattering. The latter is likely to evolve from pores that are introduced and that perform as light capturing centers as they increase the photon path throughout the electrodes. Both characteristics go hand-in-hand with an overall DSSC performance enhancement − vide infra. Quite remarkable is the fact that the implementation of SWCNHs shows the most profound impact in terms of *R* and diffuse reflectance features − Table 1 and Figure S7.

Visual corroboration of this notion came from SEM images taken for the different nanocarbon/TiO_2 photoelectrodes that, indeed, nicely confirm the differences in surface morphologies correlated with the aforementioned data. Incorporating any of the nanocarbons clearly enhances the surface porosity of the resulting films when compared to TiO_2 reference photoelectrodes – **Figure 1**. Noteworthy, the use of oxidized nanocarbons seems to have a stronger impact on the photoelectrode morphology with larger roughness factors than the addition of non-oxidized, pristine nanocarbons – Figure S8. The small crystalline size of TiO_2 particles is likely to be responsible for strong interactions with the oxidized nanocarbons and, as a consequence, films with high porosity evolve – Figure 1.

One of the major rationales for implementing nanocarbons into TiO_2 photoelectrodes is their impact on the electronic properties such as resistance and/or resistivity as well as on the work function.[5h–k] The latter was investigated using the Kelvin Probe technique – Table 1. The work function of the modified electrodes is increased with respect to the reference TiO_2 electrodes suggesting an effective incorporation of nanocarbons.[5h–k] All of the used nanocarbons feature work functions between the conduction band of TiO_2 and the FTO substrate.[5h,i,5k,15] Thus, a sufficient energy offset will not block injected electrons from diffusing to the FTO substrate. In other words, the implemented nanocarbons serve as acceptor and mediator by lowering the resistance. As a proof of concept, the resistance of our photoelectrodes is significantly reduced. For instance, the resistance of TiO_2 photoelectrodes with a thickness of 1 μm is ≈800 MΩ (Table 1).[16] Thus this value might be in the GΩ range when increasing the TiO_2 thickness as occurs for the nanocarbon/TiO_2 photoelectrodes presented in this work. In the latter, the resistances are in the range of a few hundred MΩs and, as such, attest the beneficial effects of implementing nanocarbons. The lower resistance is typically found in photoelectrodes with graphene reaching values as low as 78 MΩ in the presence of 0.5 wt%. Notable, the values that were gathered for the resistance of TiO_2 photoelectrodes with non-oxidized pristine SWCNHs were moderately low compared to those of graphene-doped electrodes – Table 1. This resistance decrease highlights the usage of graphene and SWCNHs as versatile dopants in DSSCs, since they are excellent semiconductor materials.[17] In fact, graphene and SWCNH TiO_2 composites behave similarly, that is, pristine derivatives show a resistance decrease until 0.5 wt% then an increase when amounts of 0.7 wt% are reached. In the latter case, agglomeration sets in, as *R* and diffuse reflectance indicate – vide supra. In the case of the oxidized derivatives, the film resistance remains lower than in the TiO_2 reference photoelectrodes but overall constant upon increased amounts of nanocarbons. It is likely that due to the large number of structural/electronic defects in the conjugated system, the electronic conductivity of the oxidized species is limited.[5h,18] Please note that the resistance values of SWCNTs TiO_2 composites at high implementation exceeded the detection limit of our setup. Nevertheless, our experiments indicate that an amount higher than 0.1 wt% increases the resistance, which might relate to agglomeration as previously discussed for graphene and SWCNHs.

To provide a final proof that the implementation of nanocarbons into the electrode leads to a continuous electron-conducting network that facilitates the transport of photoinjected charges and diminishes the probability of recombination process, we probed the charge recombination dynamics by means of transient absorption measurements of the different dye/electrodes in the nanosecond regime – see SI for more details. It is known that charge recombination processes are conveniently followed by monitoring the bleaching recovery at 460 nm upon 355 nm excitation.[5a,19] The spectral characteristics were similar for all the dye/electrodes with transient absorption features that agree well with the differential absorption spectrum of N719 that is attached to TiO_2 and that is oxidized, with a bleaching of the ground state metal-to-ligand charge

transfer (MLCT) and a transient absorption band at around 750 nm – Figure S9.[5a,19] Importantly, the lack of emission during the experiments and the above mentioned positive absorption band indicate effective electron injection from the excited dye. The bleaching recovery was analyzed by employing monoexponential fitting functions and the corresponding lifetimes (τ_{recom}) are listed in Table 1. In general, longer lifetimes and slower charge recombinations reflect trapping of injected electrons within the nanocarbon and, in turn, efficient transfer to FTOs. In this sense, the slow charge recombination dynamics observed in nanocarbon doped electrodes compared to TiO_2 reference devices further corroborates all of the above-mentioned trends. This finding is further corroborated by impedance experiments – vide infra.

In light of the unique electronic and morphological features of the different nanocarbon/TiO_2 films, the corresponding photoanodes emerged as promising photoelectrodes to achieve important breakthroughs in DSSC performances. To test this hypothesis, a series of DSSCs with different content of nanocarbons were fabricated and analyzed under AM 1.5 conditions – see SI. Their main characteristics are summarized in **Table 2** and depicted in **Figure 2**. A closer look at Tables 1 and 2 reveals that all of the relevant device performance features such as short-circuit current density (J_{sc}), open-circuit voltage (V_{oc}), and efficiency (η) are in line with the best aforementioned photoelectrodes. For instance, the J_{sc} trends upon nanocarbon implementation correlate with the *R* changes and/or the quantity of dye absorption as well as the enhancement of light scattering as these parameters partially govern the photocurrent generation.[5i,14] In addition, improved J_{sc}'s are also reflected in better incident monochromatic photon-to-current conversion efficiency (IPCE) performance – Figure 2. Compared to the reference devices, the IPCE response is enhanced in all of the doped electrodes leading to the same trends in the estimated short-circuit current from 11.9 to 15.7, 13.3, and 12.1 mA cm^{-2} for the reference and the doped electrodes with SWCNHs, graphene, and SWCNTs, respectively. In contrast, V_{oc}'s do not follow a clear trend and they are lower than those seen in TiO_2 reference devices. According to Kelvin Probe measurements (Table 1), this finding is not unexpected, especially considering that higher work functions are seen to evolve for modified electrodes relative to reference electrodes. Indeed, this is in line with earlier studies.[5a,5g–k] Importantly, parameters such as adsorption of additives present in the electrolyte onto the surface as well as morphological changes of the electrodes must be taken into consideration to fully understand the trends in V_{oc}.[14a,20] Nevertheless, more fascinating is the examination of the device efficiencies that are typically higher than in TiO_2 reference devices for all cases. The best values evolve for photoelectrodes doped with SWCNHs reaching efficiencies of 6.22 and 6.19% for non-oxidized, pristine and oxidized SWCNHs, respectively. Very similar are the efficiencies of 5.85 and 5.55% noted for the best devices with oxidized and pristine graphene, respectively. To verify the prospect of the best above-mentioned composites, double-layer TiO_2 electrodes were prepared to enhance the overall device performance – see SI. As a matter of fact, higher J_{sc} and FF values led to higher efficiencies. More specifically, efficiencies of 6.63, 7.98, 7.76, 7.64, and 7.45% were obtained when reference, pristine SWCNHs, oxidized SWCNHs, graphene, and partially reduced graphene oxide doped TiO_2 electrodes were utilized, respectively. These values highlight the benefits of implementing nanocarbons regarding the device performance, owing to the increase of roughness, decrease of electrical resistivity, and slow recombination dynamics – vide supra. Still, questions about the effect of the nanocarbons on the device mechanism under operation arises. To this end, we

Table 2. DSSC parameters of the different nanocarbon/TiO_2 photoelectrodes.

photoanode[a]	J_{sc} [mA cm^{-2}]	V_{oc} [V]	η [%]	*FF*
single-layer TiO_2	10.86	0.75	4.64	0.57
double-layer TiO_2	12.81	0.75	6.63	0.69
SWCNH/TiO_2				
0.1	12.14	0.68	4.87	0.59
0.2	13.47	0.71	5.55	0.58
0.5	14.68	0.73	6.22	0.58
0.5[b]	16.10	0.74	7.98	0.67
0.7	9.81	0.73	4.37	0.61
$SWCNH_{ox}$/TiO_2				
0.1	14.68	0.74	6.19	0.57
0.1[b]	15.20	0.74	7.76	0.69
0.2	14.82	0.74	6.14	0.56
0.5	12.35	0.73	5.41	0.60
0.7	9.87	0.72	4.19	0.59
graphene/TiO_2				
0.1	12.44	0.72	5.55	0.62
0.1[b]	15.01	0.76	7.64	0.67
0.2	11.19	0.71	4.69	0.59
0.5	8.78	0.71	3.86	0.62
0.7	7.17	0.7	2.86	0.57
$graphene_{ox}$/TiO_2				
0.1	11.91	0.7	4.84	0.58
0.2	13.65	0.69	5.37	0.57
0.5	14.11	0.69	5.85	0.60
0.5[b]	14.70	0.74	7.45	0.69
0.7	12.95	0.69	5.27	0.59
SWCNT/TiO_2				
0.1	12.01	0.75	5.04	0.56
0.2	5.29	0.67	2.09	0.59
0.5	4.53	0.65	1.74	0.59
0.7	4.11	0.63	1.55	0.60
$SWCNT_{ox}$/TiO_2				
0.1	12.68	0.71	5.13	0.57
0.2	8.99	0.61	3.24	0.59
0.5	4.88	0.58	1.59	0.56
0.7	3.68	0.57	1.20	0.57

[a]photoanodes were prepared using one layer of a 0.1, 0.2, 0.5 or 0.7 wt% solution of the nanocarbon/TiO_2 composites unless otherwise stated; [b]DSSCs parameters of double layer devices.

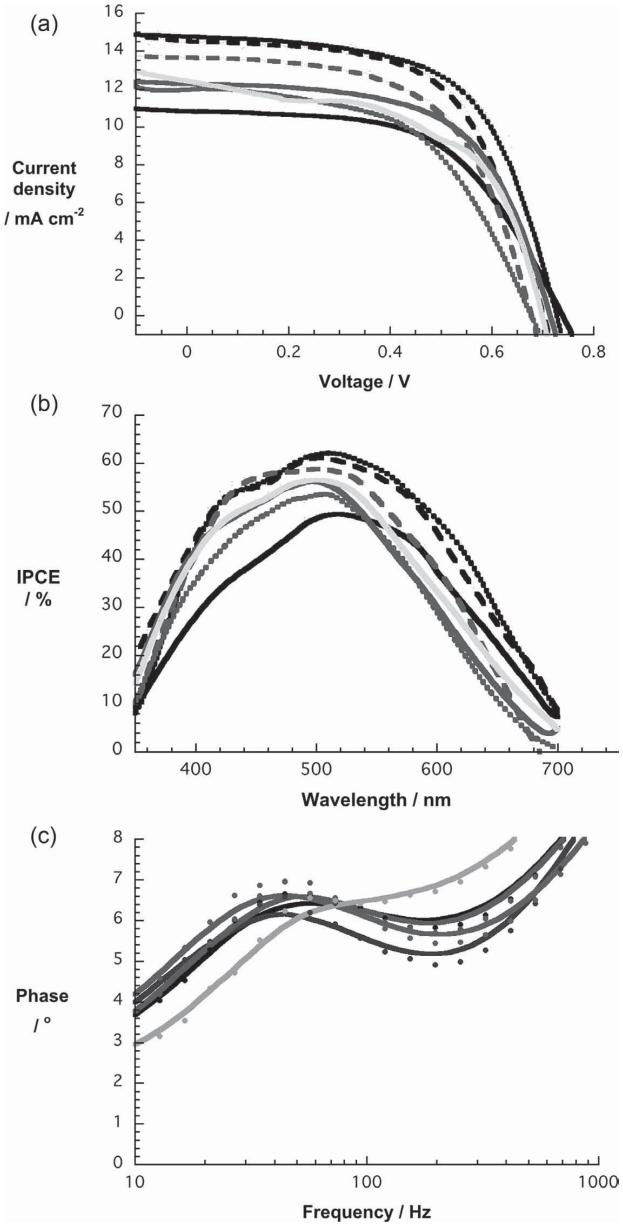

Figure 2. Upper part – *J*–*V* characteristics for DSSCs prepared with the different nanocarbon/TiO_2 photoelectrodes – reference (black solid), 0.5 wt% SWCNH (black dashed), 0.2 wt% $SWCNH_{ox}$ (black dotted), 0.1 wt% graphene (dark grey solid), 0.5 wt% $graphene_{ox}$ (dark grey dashed), 0.1 wt% SWCNT (dark grey dotted), and 0.1 wt% $SWCNT_{ox}$ (light grey solid). Central part – Incident monochromatic photo-to-current conversion efficiency (IPCE) of the different nanocarbon/TiO_2 photoelectrodes – reference (black solid), 0.5 wt% SWCNH (black dashed), 0.2 wt% $SWCNH_{ox}$ (black dotted), 0.1 wt% graphene (dark grey solid), 0.5 wt% $graphene_{ox}$ (dark grey dashed), 0.1 wt% SWCNT (dark grey dotted), and 0.1 wt% $SWCNT_{ox}$ (light grey solid). Lower part – Bode phase plot of the different nanocarbon/TiO_2 photoelectrodes under 1 sun illumination at open-circuit conditions – reference (light grey), 0.5 wt% SWCNH (grey), 0.2 wt% $SWCNH_{ox}$ (brown), 0.1 wt% graphene (black), and 0.5 wt% $graphene_{ox}$ (dark grey).

have probed the aforementioned highly efficient electrodes by means of impedance spectroscopy – more details are provided in the SI. Table S1 as well as Figures 2 and S10 summarize the most relevant figures-of-merit derived from these investigation. On one hand, studies under illumination provide information about electron transport resistance (R_w), capacitance (C), and electron lifetime (τ) and, on the other hand, studies under dark conditions shed light onto the resistance for the recombination process (R_k).[21] The combination of the R_w and R_k parameters are further used to calculate the charge collection efficiency (η_{coll}) by using the following equation:[21]

$$\eta_{coll} = 1 - (R_k/R_w) \quad (2)$$

As a matter of fact, nanocarbons as semiconductors seem to serve as electron acceptors and mediators. The latter is reflected in a reduction of R_w of around 25% as well as the increase of C by a factor of around 2.5 in the doped electrodes with respect to the reference electrodes – Table S1. As such, we conclude that the most prominent electron loss mechanism, that is, recombination, is less effective in the doped devices. This is, indeed, attested by the τ value, which increases from 2.78 (reference electrodes) to 3.6–3.9 ms (doped electrodes) – Figure 2 and Table S1 – and the R_k value, which increases from 40 (reference electrodes) to 50–60 Ω (doped electrodes) – Figure S10 and Table S1. The value of nanocarbons in the devices is also reflected in the charge collection efficiency (η_{coll}), which increases from ≈60% for the reference electrodes to ≈77% for the doped electrodes. The changes in η_{coll} point to the synergetic effects evolving from a better electron transport and a slower recombination upon implementing nanocarbons.

In summary, different nanocarbons such as SWCNTs, graphene, SWCNHs, and their respective oxidized products have been used to fabricate novel nanocarbon/TiO_2 photolectrodes for DSSCs. Our results, which are based on evaluating the roughness factor via desorption studies, diffuse reflectance, and profilometry, characterizing the morphology by means of SEM, measuring the electric resistance, assessing the dynamics for the charge recombination processes, and, ultimately, determining the device characterization and mechanism by means of impedance studies, clearly demonstrate that all of the nanocarbons significantly enhance the TiO_2 electrode characteristics and, subsequently, the photoresponse of the device with respect to standard TiO_2 electrodes. The most outstanding finding of the current work is that SWCNH derivatives are also a valuable dopant for fabricating highly efficient DSSCs.

Supporting Information

Supporting Information is available from the author.

Acknowledgements

Financial support from the Australian Research Council is gratefully acknowledged. R.D.C. acknowledges the Humboldt Foundation for its support. D.M.G. acknowledges the DFG (Cluster of Excellence – Engineering of Advanced Materials), the EU (CARINHYPH), and the ZMP for financial and intellectual support. M.A.H., M.L., and E.V. acknowledge DGICYT of Spain for funding through the project CTQ2011-22410. M.P. thanks MIUR (PRIN n. 20085M27SS and FIRB "Nanosolar" RBAP11C58Y) for financial support.

[1] a) L. J. Brennan, M. T. Byrne, M. Bari, Y. K. Gunko, *Adv. Ener. Mater.* **2011**, *1*, 472; b) S. Zhu, G. Xu, *Nanoscale* **2010**, *2*, 2538; c) D. M. Guldi, V. Sgobba, *Chem. Commun.* **2011**, *47*, 606; d) Y. Sun, Q. Wu, G. Shi, *Energy Environ. Sci.* **2011**, *4*, 1113.

[2] A. Yella, H.-W. Lee, H. N. Tsao, C. Yi, A. K. Chandiran, M. K. Nazeeruddin, E.W.-G. Diau, C. Y. Yeh, S. M. Zakeeruddin, M. Grätzel, *Science* **2011**, *334*, 629.

[3] a) B. O'Reagan, M. Grätzel, *Nature* **1991**, *353*, 737; b) A. Hagfeldt, G. Boschloo, L. Sun, L. Kloo, H. Pettersson, *Chem. Rev.* **2010**, *110*, 6595.

[4] M. K. Nazeeruddin, E. Baranoff, M. Grätzel, *Solar Energy* **2011**, *85*, 1172.

[5] a) P. Brown, K. Takechi, P. V. Kamat, *J. Phys. Chem. C* **2008**, *112*, 4776; b) A. Du, Y. H. Ng, N. J. Bell, Z. Zhu, R. Amal, S. C. Smith, *J. Phys. Chem. Lett.* **2011**, *2*, 894; c) H.-I. Kim, G.-H. Moon, D. Monllor-Satoca, Y. Park, W. Choi, *J. Phys. Chem. C* **2012**, *116*, 1535; d) S. L. Kim, S.-R. Jang, R. Vittal, J. Lee, K.-J. Kim, *J. Appl. Elec.* **2006**, *36*, 1433; e) S. R. Kim, M. K. Parvez, M. Chhowalla, *Chem. Phys. Lett.* **2009**, *483*, 124; f) A. Kongkanand, R. Martinez-Dominguez, P. V. Kamat, *Nano Lett.* **2007**, *7*, 676; g) J. Song, Z. Yin, Z. Yang, P. Amaladass, S. Wu, J. Ye, Y. Zhao, W.-Q. Deng, H. Zhang, X.-W. Liu, *Chem. Eur. J.* **2011**, *17*, 10832; h) Y. B. Tang, C. S. Lee, J. Xu, Z. T. Liu, Z. H. Chen, Z. He, Y. L. Cao, G. Yuan, H. Song, L. Chen, L. Luo, H. M. Cheng, W. J. Zhang, I. Bello, S. T. Lee, *ACS Nano* **2010**, *4*, 3482; i) N. Yang, J. Zhai, D. Wang, Y. Chen, L. Jiang, *ACS Nano* **2010**, *4*, 887; j) C.-Y. Yen, Y.-F. Lin, S.-H. Liao, C.-C. Weng, C.-C. Huang, Y.-H. Hsiao, C.-C.M. Ma, M.-C. Chang, H. Shao, M.-C. Tsai, C.-K. Hsieh, C.-H. Tsai, F.-B. Weng, *Nanotechnology* **2008**, *12*, 375305; k) S. Sun, L. Gao, Y. Liu, *App. Phys. Lett.* **2010**, *26*, 083113.

[6] a) I. Ahmad, U. Khan, Y.K. Gun'ko, *J. Mater. Chem.* **2011**, *21*, 16990; b) N. Ikeda, T. Miyasaka, *Chem. Lett.* **2007**, 466; c) C.-P. Lee, L.-Y. Lin, P.-Y. Chen, R. Vittal, K.-C. Ho, *J. Mater. Chem.* **2010**, *20*, 3619.

[7] a) L. Kavan, J.-H. Yum, M. Grätzel, *Nano Lett.* **2011**, *11*, 5501; b) L. Kavan, J.-H. Yum, M. K. Nazeeruddin, M. Grätzel, *ACS Nano* **2011**, *5*, 9171; c) D. W. Zhang, X. D. Li, H. B. Li, S. Chen, Z. Sun, X. J. Yin, S. M. Huang, *Carbon* **2011**, *42*, 5382.

[8] a) S. Iijima, M. Yudasaka, R. Yamada, S. Bandow, K. Suenaga, F. Kokai, K. Takahshi, *Chem. Phys. Lett.* **1999**, *302*, 165; b) T. Azami, D. Kasuya, R. Yuge, M. Yudasaka, S. Iijima, T. Yoshitake, Y. Kubo, *J. Phys. Chem. C* **2008**, *112*, 1330.

[9] a) E. Sani, L. Mercatelli, S. Barison, C. Pagura, F. Agresti, L. Colla, P. Sansoni, *Sol. Energy Mater. Sol. Cells* **2011**, *25*, 2994; b) A. Izadi-Najafabadi, T. Yamada, D. N. Futaba, M. Yudasaka, H. Takagi, H. Hatori, S. Iijima, K. Hata, *ACS Nano* **2011**, *5*, 811.

[10] a) G. Pagona, A. S. D. Sandanayaka, T. Hasobe, G. Charalambidis, A. G. Coutsolelos, M. Yudasaka, S. Iijima, N. Tagmatarchis, *J. Phys. Chem. C* **2008**, *112*, 15735; b) M. Vizuete, M.J. Gómez-Escalonilla, J. L. G. Fierro, A. S. D. Sandanayaka, T. Hasobe, M. Yudasaka, S. Iijima, O. Ito, F. Langa, *Chem. Eur. J.* **2010**, *16*, 10752.

[11] a) C. Cioffi, S. Capidelli, C. Sooambar, M. Marcaccio, G. Marcolongo, M. Meneghetti, D. Paoluccio, F. Paoluccio, C. Ehli, G. M. A. Rahman, V. Sgobba, D. M. Guldi, M. Prato, *J. Am. Chem. Soc.* **2007**, *122*, 3938; b) Y.-F. Li, C.-L. Lu, S.-L. Kuo, S.-C. Huang, B.-Y. Wei, S.-C. Chang, W.-K. Hsu, *J. Mater. Chem.* **2011**, *21*, 2178; c) J. Yan, Z. Zhao, L. Pan, *Phys. Status Solidi A* **2011**, *208*, 2335.

[12] B. Tan, Y. Wu, *J. Phys. Chem. B* **2006**, *110*, 15932.

[13] M. Grätzel, *Pure Appl. Chem.* **2001**, *73*, 459.

[14] a) T. T. T. Pham, T. Bessho, N. Mathews, S. M. Zakeeruddin, Y. M. Lam, S. Mhaisalkar, M. Grätzel, *J. Mater. Chem.* **2012**, *22*, 16201; b) S. Hore, P. Nitz, C. Vetter, C. Prahl, M. Niggermann, R. Kern, *Chem. Commun.* **2005**, 2011.

[15] a) M. Grätzel, *Nature* **2001**, *414*, 338; b) D. V. Kolesnikow, V. A. Osipov, *JETP Letters* **2004**, *72*, 660; c) C. Chen, W. Cai, M. Long, B. Zhou, Y. Wu, D. Wu, Y. Feng, *ACS Nano* **2010**, *4*, 6425; d) H. Ago, T. Kugler, F. Cacialli, W. R. Salaneck, M. S. P. Schaffer, A. H. Windle, R. H. Friend, *J. Phys. Chem. B* **1999**, *103*, 8116; e) R. Czwer, B. Foley, D. Tekleab, A. Rublo, P. M. Ajayan, *Phys. Rev. B* **2002**, *66*, 033408.

[16] I. Senain, N. Nayan, H. Saim, *Int. J. Integ. Engin.* **2011**, 29.

[17] K. Urita, S. Seki, S. Utsumi, D. Noguchi, H. Kanoh, H. Tanaka, Y. Hattoti, Y. Ochiai, N. Aoki, M. Yudasaka, S. Iijima, K. Kaneko, *Nano Lett.* **2006**, *6*, 1325.

[18] I. Jung, D. A. Dikin, R. D. Piner, R. S. Ruoff, *Nano Lett.* **2008**, *8*, 4283.

[19] a) A. Listorti, B. O'Regan, J. R. Durrant, *Chem. Mater.* **2011**, *23*, 3381; b) R. W. Fessenden, P. V. Kamat, *J. Phys. Chem.* **1995**, *22*, 12902.

[20] a) S. Zhang, X. Yang, K. Zhang, H. Chen, M. Yanagida, L. Han, *Phys. Chem. Chem. Phys.* **2011**, *13*, 19310; b) S. E. Koops, B. C. ORegan, P. R. F. Barnes, J. R. Durrant, *J. Am. Chem. Soc.* **2009**, *131*, 4808.

[21] a) M. Adachi, M. Sakamato, J. Jiu, Y. Ogata, S. Isoda, *J. Phys. Chem. B* **2006**, *110*, 13872; b) Q. Wang, Z. Zhang, S. M. Zakeeruddin, M. Grätzel, *J. Phys. Chem. C* **2008**, *112*, 7084.